

Mantle solidus: Experimental constraints and the effects of peridotite composition

Marc M. Hirschmann

Department of Geology and Geophysics, University of Minnesota, Minneapolis, Minnesota 55455
(Marc.M.Hirschmann-1@umn.edu)

[1] **Abstract:** A review of experiments on natural peridotites allows improved constraints on the location of the mantle solidus. Available constraints on the location of the nominally dry peridotite solidus show considerable scatter, owing to interlaboratory uncertainties and the effects of bulk composition. When experiments on enriched peridotite are filtered from the database, the best fit to the solidus between 0 and 10 GPa is given by $T(^{\circ}\text{C}) = aP^2 + bP + c$ where $a = -5.104$, $b = 132.899$, and $c = 1120.661$ and P is in gigapascals. Compared to previous models, the solidus in this parameterization is at lower temperature between 2 and 6 GPa, with the largest differences near 4 GPa, where it is $30^{\circ} - 60^{\circ}\text{C}$ cooler. Consideration of experimental constraints on the peridotite solidus and of a theoretical model of melting in a simple analogue system suggests that a key variable affecting peridotite solidus temperature is the near-solidus liquid alkali concentration. The effect of alkalis on the solidus increases with bulk concentration in the peridotite but decreases with bulk partition coefficient. Thus small bulk concentrations of K can have a significant influence on the peridotite solidus, and the effect of Na diminishes with increasing pressure, as it becomes more compatible in the solidus residua. $\text{Mg \#} [=100 \times \text{MgO}/(\text{MgO} + \text{FeO})]$ variations are subordinate to alkali variations in controlling solidus temperature at lower pressures but may increase in relative importance as alkalis become more compatible in peridotite residua with increasing pressure. Increased clinopyroxene mode has the effect of making Na more compatible in residual solids and so diminishes the solidus-lowering tendencies of alkalis. As a consequence, experiments performed on a range of peridotite compositions may not reflect the likely effect of variable mantle composition on solidus temperature if they do not match the appropriate correlation between alkali content and clinopyroxene mode.

Keywords: Peridotite; melting; high-pressure experiments; mantle; solidus.

Index terms: Experimental mineralogy and petrology; igneous petrology; high-pressure behavior; major element composition.

Received March 25, 2000; **Revised** August 21, 2000; **Accepted** September 13, 2000; **Published** October 24, 2000.

Hirschmann, M. M., 2000. Mantle solidus: Experimental constraints and the effects of peridotite composition, *Geochem. Geophys. Geosyst.*, vol. 1, Paper number 2000GC000070 [11,012 words, 12 figures, 3 tables]. Published October 24, 2000.

Theme: Phase Relations and Trace Element Partitioning on the Mantle Solidus

Guest Editors: Vincent Salters and Jon Blundy

1. Introduction

[2] The location of the peridotite solidus is a critical parameter influencing the geodynamics of partial melt formation in the mantle. The solidus location is a fundamental constraint on the initial depth of melting for upwelling mantle beneath oceanic ridges and elsewhere, and the solidus position, combined with observations of oceanic crust thickness and composition, yields a crucial bound on the potential temperature of the present-day convecting mantle [e.g., *McKenzie*, 1984]. However, owing to experimental uncertainties and the effects of variable peridotite composition, the solidus of mantle peridotite remains imperfectly constrained.

[3] The effect of peridotite composition on the location of the peridotite solidus is poorly resolved at present. Although modelers have considered the likely effect of peridotite composition on the production and composition of partial melts produced [e.g., *Langmuir et al.*, 1992; *Shen and Forsyth*, 1995], there are relatively few experimental studies that quantify the compositional influences on the onset of melting [*Robinson et al.*, 1998; *Pickering-Witter and Johnston*, 2000; *Schwab and Johnston*, 2000]. However, the recent increase in available experimental data on a range of peridotite compositions allows a more comprehensive evaluation of the role of composition on the solidus.

[4] The aim of this paper is to examine the position of the volatile-absent peridotite solidus. Small quantities of CO₂, H₂O, and other volatiles likely result in small degrees of melting of the mantle at temperatures less than the dry solidus [*Galer and O'Nions*, 1986; *Plank and Langmuir*, 1992; *Langmuir et al.*, 1992; *Hirth and Kohlstedt*, 1996; *Karato and Jung*, 1998], but the volatile-free solidus remains an important end-member

constraint on partial melting processes, particularly because the volumes of melt produced by trace volatile constituents are relatively small. Also, experimental data are at this time insufficient to parameterize accurately the effect of trace volatile constituents. On the other hand, experiments designed to examine partial melting of dry peridotite may well be unintentionally influenced by small quantities of volatiles [e.g., *Hirschmann et al.*, 1998; *Holloway*, 1998]. For this reason, the experiments examined in this paper are judged to be nominally dry, and departures from true dry conditions are considered as one of several possible experimental imperfections that affect solidus determinations. This paper builds on earlier parameterizations of the peridotite solidus [*McKenzie and Bickle*, 1988; *Langmuir et al.*, 1992; *Iwamori et al.*, 1995] and is in many respects similar to the new treatment of *Herzberg et al.* [2000] but considers a wider range of experimental data and presents a more extensive discussion of the effect of peridotite composition.

2. Experimental Database

[5] In this paper we consider experimental data that constrain the nominally dry peridotite solidus between 0 and 10 GPa collected with either piston cylinder or multianvil apparatuses (Table 1). We focus on compositions approximating natural terrestrial peridotite and unless otherwise noted do not consider extraterrestrial peridotite compositions [*Bertka and Holloway*, 1994; *Agee et al.*, 1995] or synthetic analogues with simplified compositional components [e.g., *Walter and Presnall*, 1994; *Gudfinnsson and Presnall*, 2000]. The studies in the newly compiled database include 30 melt-absent experiments and 82 melt-present experiments (Table 1). These data are plotted in Figure 1, along with the 70 constraints compiled by *McKenzie and Bickle* [1988]. The combined constraints comprise 135 data points between

Table 1. Sources of Post-1988 Constraints on Peridotite Solidus

Source	Melt Absent	Melt Present
<i>Baker et al.</i> [1995]	1	1
<i>Canil</i> [1992]		4
<i>Falloon and Green</i> [1988]		8
<i>Falloon et al.</i> [1988]	2	4
<i>Falloon et al.</i> [1999]	4	2
<i>Herzberg et al.</i> [2000]	2	3
<i>Hirose and Kushiro</i> [1993]		10
<i>Iwamori et al.</i> [1995] ^a	2	8
<i>Kushiro</i> [1996]		6
<i>Pickering-Witter and Lesher</i> [1999]	1	1
<i>Pickering-Witter and Johnston</i> [2000]		4
<i>Robinson and Wood</i> [1998]	1	7
<i>Robinson et al.</i> [1998]	1	2
<i>Schwab and Johnston</i> [2000]	2	5
<i>Takahashi et al.</i> [1993]	5	6
<i>Walter</i> [1998]	6	6
<i>Yaxley</i> [2000]	1	1
<i>Zhang and Herzberg</i> [1994] ^b	2	4
Total	30	82

^aUnpublished data of Shimazaki and Shimazaki and Takahashi, cited by *Iwamori et al.* [1995].

0.1 MPa and 3.5 GPa but only 47 between 3.5 and 10 GPa. Also, constraints on the solidus above 3.5 GPa are less robust because of difficulties calibrating temperature and pressure under more extreme conditions.

3. Preliminary Estimated Solidus for Mantle Peridotite

[6] The temperature-pressure path of the solidus in complex systems can be estimated from the specific volumes and entropies of the liquid present along the solidus and from the partial specific volume and entropy of the liquid components in the equilibrium solidus crystalline assemblage [*Walker et al.*, 1988]. Thus, given sufficiently accurate information about the solidus liquid and residual mineral compositions and the thermodynamic properties of the constituent

phases, the solidus of a peridotite may be calculated. However, because near-solidus solid and liquid compositions vary in a complex fashion with increasing pressure, there is no simple rigorous analytical function that describes the temperature-pressure path of the peridotite solidus. *Asimow et al.* [2000] used thermodynamic data to locate the solidus implicitly with the MELTS algorithm. This calculation shows reasonable agreement with experimental determinations of the peridotite solidus but does not provide the most accurate possible description of the solidus.

[7] To parameterize the solidus, we adopt a simple polynomial relationship between temperature and pressure

$$T_{\text{solidus}} = aP^2 + bP + c, \quad (1)$$

where pressure is given in gigapascals and a , b , and c are regressed constants. We have also examined more complex polynomials and functions using logarithmic or reciprocal functions of pressure, but these gave no appreciable improvement in fit relative to this simple polynomial. Note that this parameterization does not take into account theoretically required inflections associated with transitions between plagioclase, spinel, and garnet peridotite [*Presnall*, 1969]; these inflections cannot at this time be resolved within interlaboratory experimental uncertainty.

[8] The available data include contradictory constraints, with some studies reporting sub-solidus conditions at similar pressure but higher temperatures than other studies reporting melt present (Figure 1). If the sources of scatter in the data can be treated as random experimental errors (i.e., rather than owing to systematic interlaboratory biases owing to compositional dependencies), then the best estimate of the peridotite solidus that can be obtained from these data in aggregate is a function that mini-

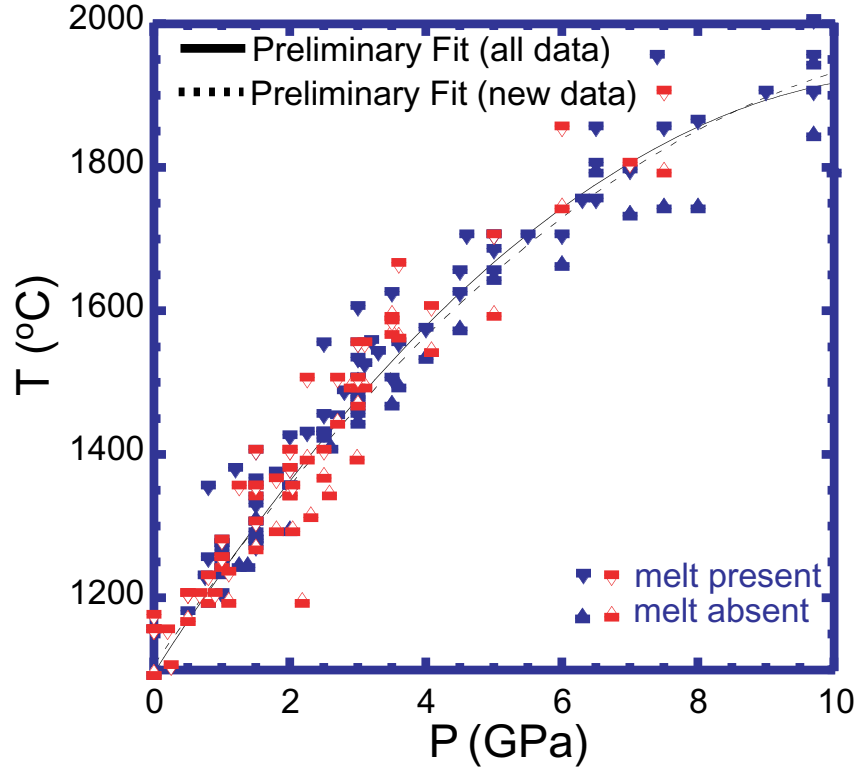


Figure 1. Experimental constraints on the solidus of natural peridotite. Arrows pointing down are experiments in which melt was detected; those pointing up are subsolidus experiments. Solid symbols are from the post-1988 compilation in this paper (references in Table 1); open symbols are from the pre-1988 compilation of *McKenzie and Bickle* [1988]. Best fits to these data, discussed in the text, include the best fit to all the data (solid curve), the best fit to the post-1988 data (dashed line).

minimizes violations of the available constraints. To do so, we construct a penalty function that is the sum of the square of temperature discrepancies for those points that violate the function. In other words, a solution is sought such that X^2 is minimized, where X^2 is given by

$$X^2 = \tau n_s \perp n = 1 \sum x_i^s + \tau n_l \perp n = 1 \sum x_i^l \quad (2)$$

and where n_s and n_l are the number of experimental observations below and above the peridotite solidus respectively, x_i^s and x_i^l are given by

$$x_i^s = \begin{cases} 0; & T_{\text{model}}^P > T_{\text{melt-absent}}^P \\ (T_{\text{model}}^P - T_{\text{melt-absent}}^P)^2; & T_{\text{model}}^P < T_{\text{melt-absent}}^P \end{cases} \quad (3a)$$

$$x_i^l = \begin{cases} (T_{\text{model}}^P - T_{\text{melt-present}}^P)^2; & T_{\text{model}}^P > T_{\text{melt-present}}^P \\ 0; & T_{\text{model}}^P < T_{\text{melt-present}}^P \end{cases} \quad (3b)$$

and T_{model}^P , $T_{\text{melt-absent}}^P$, and $T_{\text{melt-present}}^P$ are the temperatures predicted by the model, of melt-absent, and of melt-present experiments, respectively. The best fit is found iteratively, using Newton's method. Coefficients for the solutions for both the complete data set and the post-1988 data are given in Table 2 and graphically illustrated in Figure 1. These solutions give similar P - T trends for the peridotite solidus, with a maximum difference near 4 GPa, where the new data alone lead to a solidus $\sim 15^\circ\text{C}$ cooler than the complete data set.

Table 2. Parameterizations of the Peridotite Solidus

	All Data	Post-1988 Data	Recommended Fit ^b	NoMPY ^c
Filtered for composition?	no	no	yes	yes
<i>Coefficients</i>				
a ($^{\circ}\text{C}/\text{GPa}^2$) ^a	-6.435	-5.315	-5.1404654	-5.722
b ($^{\circ}\text{C}/\text{GPa}$) ^a	146.533	135.675	132.899012	137.863
c ($^{\circ}\text{C}$) ^a	1096.154	1107.113	1120.66061	1124.123
<i>Constraints</i>				
n (total)	180	122	63	49
n_s (melt-absent)	54	30	19	16
n_l (melt present)	103	82	44	33
χ^2	3.22E+04 ^d	1.43E+04	7.60E+03	4.22E+03

^aCoefficients to expression $T = aP^2 + bP + c$.

^bFit to post-1988 data with enriched and depleted peridotite compositions removed.

^cSimilar to recommended fit, but with MPY and similar compositions excluded (see text).

^dRead 3.22E+04 as 3.22×10^4 .

4. Experimental Uncertainties

[9] The scatter in solidi evident in Figure 1 derives in part from experimental uncertainties associated with solidus location and in part from effects attributable to variations in peridotite bulk composition. Experimental uncertainties include inaccuracies in sample temperature and pressure determinations in solid media pressure devices and imperfect control on bulk composition, owing to loss of Fe either from the charge to Pt containers or to small quantities of volatile components inadvertently introduced with the sample capsule or by diffusion through the sample capsule during the experiment.

[10] Another important factor contributing to differences between experimental results is the experimental procedure. For conventional melting experiments, small degree melts may not quench to a glass, particularly at high pressures where melts have very low viscosity. On the other hand, melt may persist below the peridotite solidus in peridotite-basalt sandwich experiments if the initial basalt composition differs from the composition of the equilibrium near-solidus liquid. Thus procedural imperfections may cause either underestimates or overestimates of solidus temperature.

[11] An interesting example of the uncertainties associated with interlaboratory determinations of the solidus comes from two independent studies of the same peridotite, KLB-1, at 1.5 GPa [Takahashi *et al.*, 1993; Hirose and Kushiro, 1993]. The starting material used in both studies is reputedly from the same bottle of powder (T. Kogiso, personal communication, 1999), so differences in result must be attributable to laboratory methods. Takahashi *et al.* [1993] report melt absent at 1350 $^{\circ}\text{C}$ and melt present at 1400 $^{\circ}\text{C}$. A least squares fit to temperature versus melt fraction (F) for these experiments yields an intercept of $1349 \pm 28^{\circ}\text{C}$ ($n = 3$), so 1350 $^{\circ}\text{C}$ is a reasonable estimate of the solidus temperature (Figure 2). In contrast, Hirose and Kushiro [1993] report melt at 1300 $^{\circ}\text{C}$, and though the solidus was not determined directly, linear extrapolation of the temperature versus melt fraction trend suggests a solidus of $1292 \pm 7^{\circ}\text{C}$, $\sim 60^{\circ}\text{C}$ lower than that indicated by Takahashi *et al.* [1993]. Note that Hirose and Kushiro [1993] estimated melt fraction by assuming that Na is perfectly incompatible. Because this is not strictly true, this procedure must overestimate melt fraction. We have revised these melt fraction estimates by assuming realistic values for D_{Na} (details are in caption to Figure 2). The discrepancy

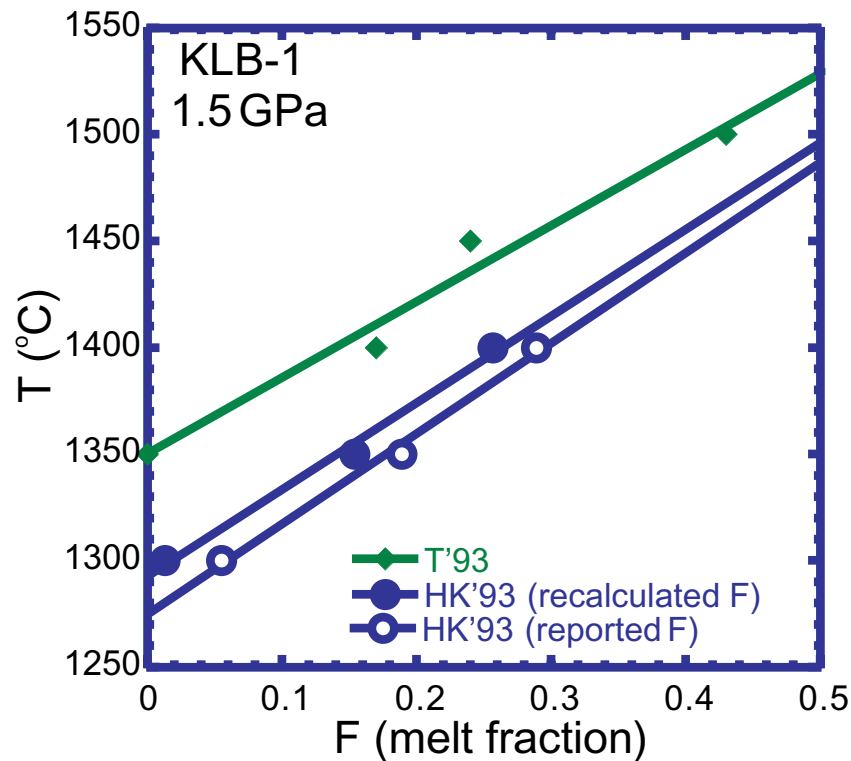


Figure 2. Temperature versus melt fraction for partial melting of experiments at 1.5 GPa by *Takahashi et al.* [1993] and by *Hirose and Kushiro* [1993]. Melt fractions for *Hirose and Kushiro* [1993] are revised from that reported in their study. *Hirose and Kushiro* [1993] estimated melt fractions based on the assumption that Na is completely incompatible, which has the tendency of exaggerating the actual melt fraction present. Revised estimates of melt fraction are based on the batch melting equation, using reported Na_2O concentrations in glasses and KLB-1 bulk composition, estimates for D_{Na} in clinopyroxene (cpx) and orthopyroxene (0.2 and 0.05, respectively) appropriate for near-solidus partial melting of fertile peridotite [Robinson *et al.*, 1998], and the bulk cpx and opx modes (cpx = 0.15, opx = 0.25) for KLB-1 reported by *Hirose and Kushiro* [1993]. Trends for temperature versus melt fraction data are fit using linear least squares, with extrapolated solidi of $1350 \pm 28^\circ\text{C}$ [Takahashi *et al.*, 1993], $1292 \pm 7^\circ\text{C}$ [Hirose and Kushiro, 1993, with revised melt fractions], and $1275 \pm 7^\circ\text{C}$ [Hirose and Kushiro, 1993, with reported melt fractions]. Although linear extrapolation of temperature-melt fraction trends are not theoretically justified, owing to expected nonlinearities associated with clinopyroxene exhaustion and with near-solidus steepening of the T versus F curve [Hirschmann *et al.*, 1999], the likely error associated with the assumption of linearity may be small when data at low melt fraction are available.

between the two different studies is 75°C if Hirose and Kushiro's estimates are used (Figure 2).

[12] The cause of the differences in these two partial melting studies is unknown, but it is probably significant that the respective temperature versus melt fraction trends are nearly

parallel (Figure 2). Experimental uncertainties that could potentially affect melt fraction estimates, such as Fe loss, volatile contamination, experimental design, or method of melt fraction determination, are likely to vary with temperature or melt fraction. This suggests that the chief difference in the two studies is temperature and/or pressure calibration.

Table 3. Compositions of Selected Peridotites

	"Bristol"		"Tokyo"			
	MPY ^a	T ⁷ quillo ^a	KLB-1 ^b	HK-66 ^b	PHN-1611 ^c	KR4003 ^d
SiO ₂	44.7	44.9	44.48	48.02	43.7	44.9
TiO ₂	0.17	0.08	0.16	0.22	0.25	0.16
Al ₂ O ₃	4.37	3.22	3.59	4.88	2.75	4.26
Cr ₂ O ₃	0.45	0.28	0.31	0.25	0.28	0.41
FeO*	7.55	7.58	8.1	9.9	10.05	8.02
MnO			0.12	0.14	0.13	0.13
MgO	38.6	40	39.22	32.35	37.22	37.3
CaO	3.38	2.99	3.44	2.97	3.26	3.45
Na ₂ O	0.4	0.18	0.3	0.66	0.33	0.22
K ₂ O			0.03	0.07	0.14	0.09
	99.62	99.23	99.75	99.46	98.11	98.94
Mg # ^e	90.1	90.4	89.6	85.3	86.8	89.2

^aRobinson and Wood [1998].

^bHirose and Kushiro [1993].

^cKushiro [1996].

^dWalter [1998].

^eMg # = 100 × molar Mg/(Mg + Fe) with all Fe as Fe²⁺.

[13] The ~60°C difference in solidi between these two studies may be greater than the usual magnitude of interlaboratory uncertainties. For example, consistency between the solidus determinations of *Pickering-Witter and Johnston* [2000] and *Baker et al.* [1995] suggest interlaboratory reproducibility of close to 10°C. On the other hand, *Longhi* [1998] has shown at least one case in which the interlaboratory discrepancy in solidus location for a CMAS peridotite analogue is close to 100°C.

5. Effect of Peridotite Composition

[14] Variations in peridotite composition are likely to be responsible for some of the scatter in experimental peridotite solidus locations (Figure 1) and also for variations in partial melting behavior of peridotite in the mantle. The most commonly considered compositional controls on the nominally dry peridotite solidus temperature are the Mg # and alkali contents, but it will be argued below that CaO, which affects the modal proportions of cpx, is also important.

[15] Because of interlaboratory uncertainties in solidus determination, the effects of composition on the peridotite solidus can best be evaluated by studies performed in the same laboratory by the same methods. Comparison of intralaboratory results minimizes uncertainties caused by imperfections in experimental technique. Here we consider results from three different sets of studies that yield constraints on the effects of peridotite composition: (1) experiments at 1.5 and 3 GPa using the diamond aggregate method on KLB-1, HK-66, and PHN-1611 peridotite [*Hirose and Kushiro*, 1993; *Kushiro*, 1996], (2) experiments at 1.5 GPa and near 3 GPa using direct partial melting and sandwich techniques on mid-ocean ridge basalt (MORB) pyrolite (MPY) and Tinaquillo lherzolite [*Robinson et al.*, 1998; *Robinson and Wood*, 1998], and (3) experiments at 1 GPa using diamond aggregate and vitreous carbon melt traps on a range of peridotite compositions constructed from varying modal proportions of peridotitic mineral separates [*Baker and Stolper*, 1994; *Baker et al.*, 1995; *Pickering-Witter and Johnston*, 2000; *Schwab and Johnston*,

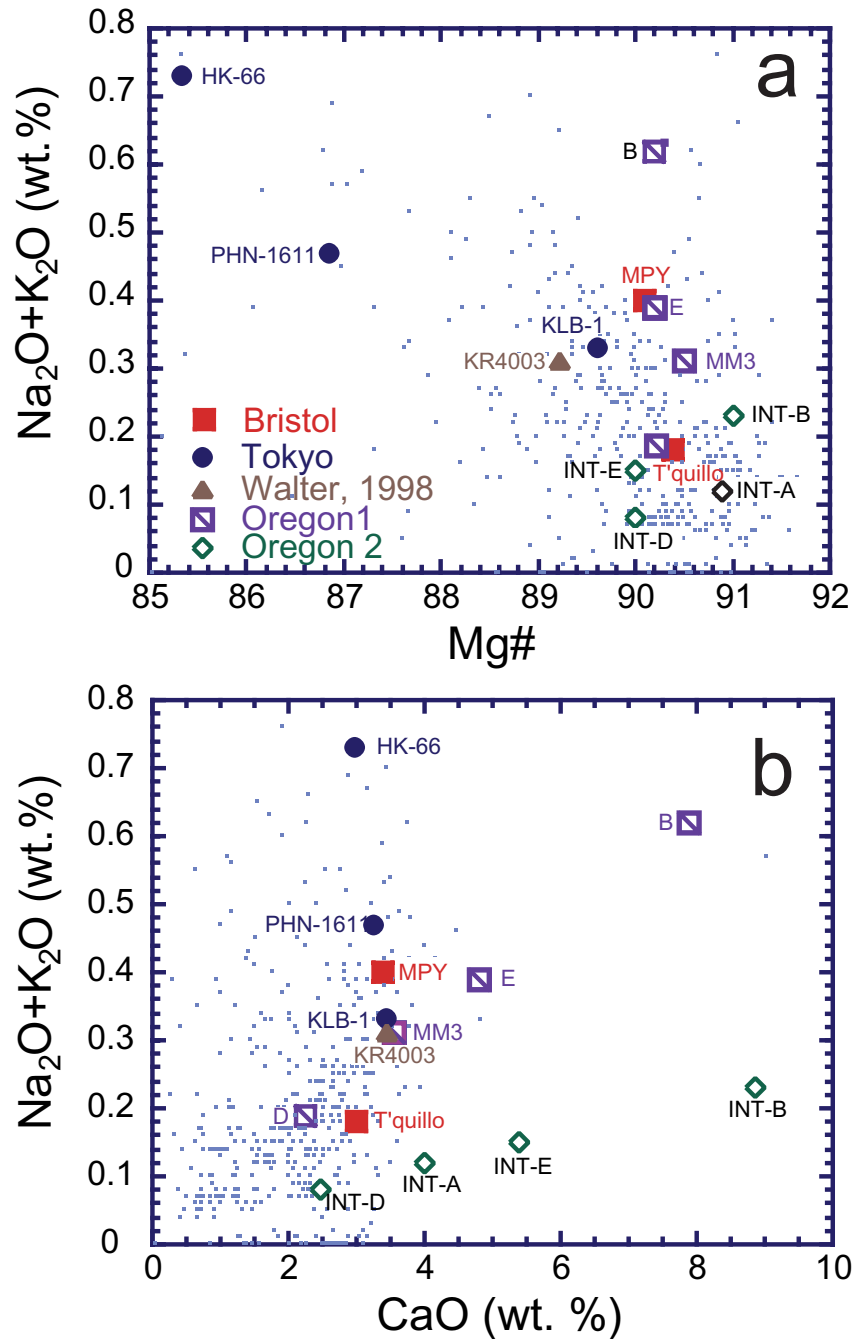


Figure 3. (a) Mg # versus total wt % alkalis and (b) CaO wt % versus total wt % alkalis for compositions of peridotite used for experiments reviewed in this study. Groups of compositions (and experimental pressures examined) include “Oregon1” (1 GPa): (B, D, E) *Pickering-Witter and Johnston* [2000] and MM3 [*Baker and Stolper*, 1994], “Oregon2” (1 GPa): INT-A, INT-B, INT-D, and INT-E [*Schwab and Johnston*, 2000], “Bristol” (1.5 and 3 GPa): MPY and Tinaquillo [*Robinson and Wood*, 1998], and “Tokyo” (1.5 and 3 GPa) KLB-1, HK-66 [*Hirose and Kushiro*, 1993], and PHN-1611 [*Kushiro*, 1996]. Light grey stipples are compositions of peridotite xenoliths from the compilation of *Herzberg et al.* [1988].

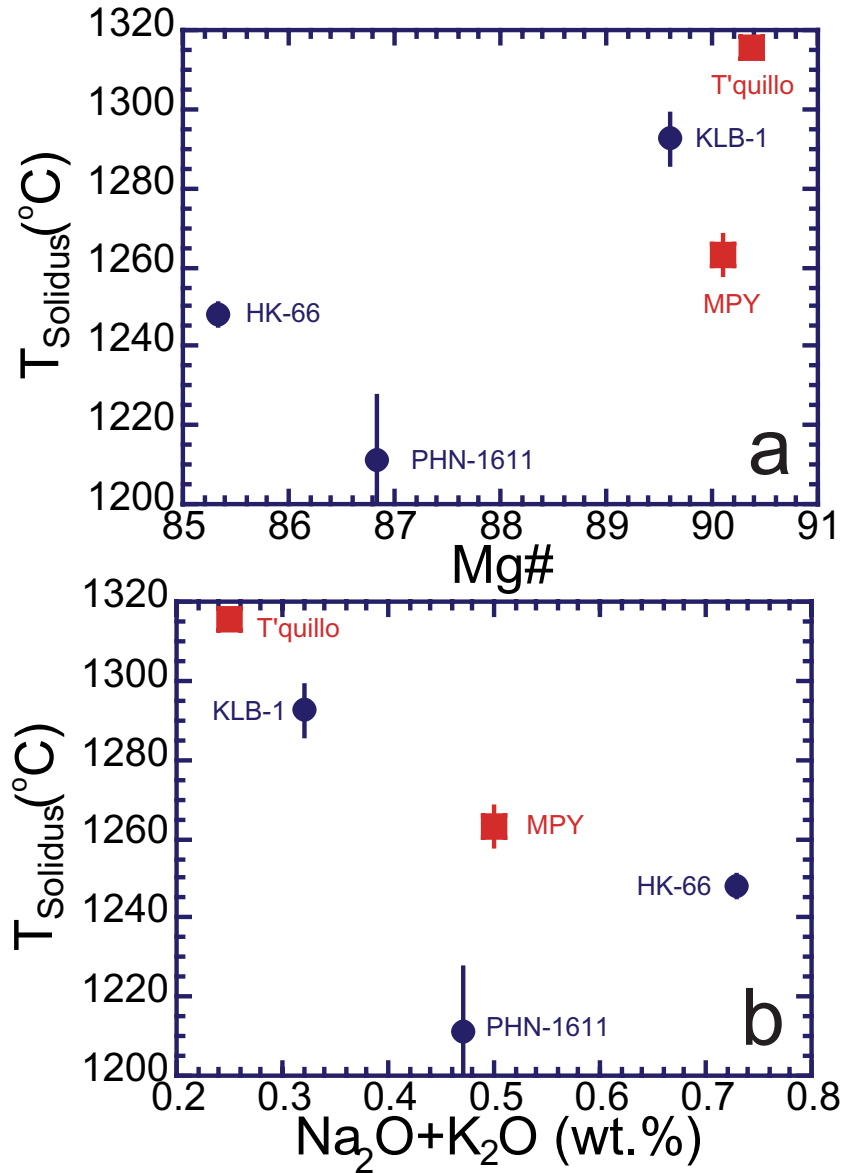


Figure 4. Comparison of solidus temperatures for several peridotite bulk compositions at 1.5 GPa versus (a) Mg # and (b) bulk alkalis in wt %. Solidi are taken from linear extrapolation of temperature versus melt fraction data, with 2σ errors of regression shown. For Tokyo experiments, melt fractions are recalculated as described in caption to Figure 2, using bulk cpx and opx modes for HK-66 of 0.14 and 0.66 [Hirose and Kushiro, 1993]. As actual modes for PHN-1611 are not known, they are assumed to be the same as for KLB-1 modes [Hirose and Kushiro, 1993], based on similar MgO/SiO_2 and CaO for these two compositions (Table 3). Bulk compositions of Tinaquillo and MPY peridotites are taken from Robinson and Wood [1998] and are believed to be more accurate than those given by Robinson *et al.* [1998; J. Blundy, written communication, 2000].

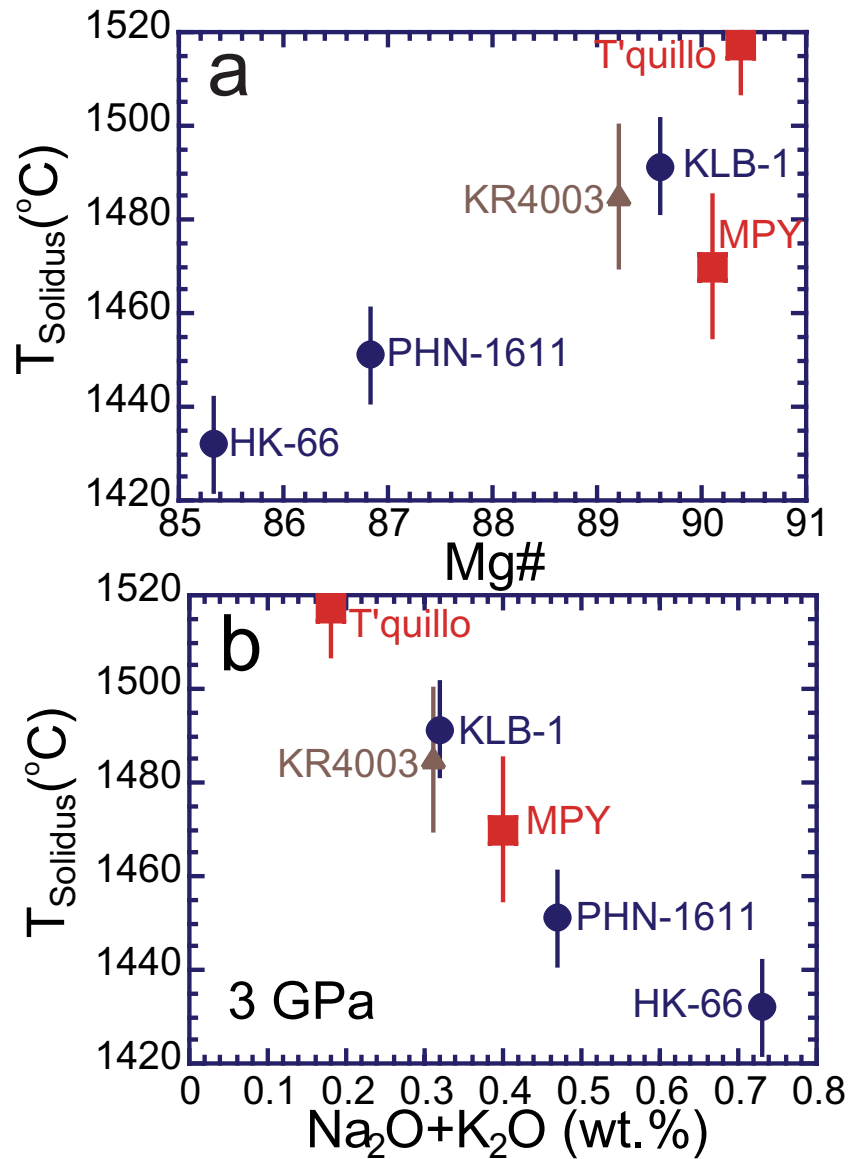


Figure 5. Comparison of solidus temperatures for several peridotite bulk compositions at 3 GPa versus (a) Mg # and (b) bulk alkalis in wt %. Solidi for Tinaquillo and MPY peridotites are taken from near-solidus brackets given by *Robinson and Wood* [1998]. Solidi for KLB-1, HK-66, and PHN-1611 are as in Figures 2 and 4, *Hirose and Kushiro* [1993] and *Kushiro* [1996] with melt fraction recalculated as described in captions to Figures 2 and 4, using $D_{\text{Na}}^{\text{cpx/liq}}$ and $D_{\text{Na}}^{\text{opx/liq}}$ of 0.48 and 0.13 [*Walter*, 1998] and mineral modes given in caption to Figure 4. Solidus for KR4003 is taken from linear extrapolation of temperature versus melt fraction data reported by *Walter* [1998]. Error bars are either 2σ from linear extrapolation or estimated from location of melt present and melt absent constraints. At 3 GPa, KR4003 and MPY are in the garnet facies, but the other peridotites have spinel peridotite residua.

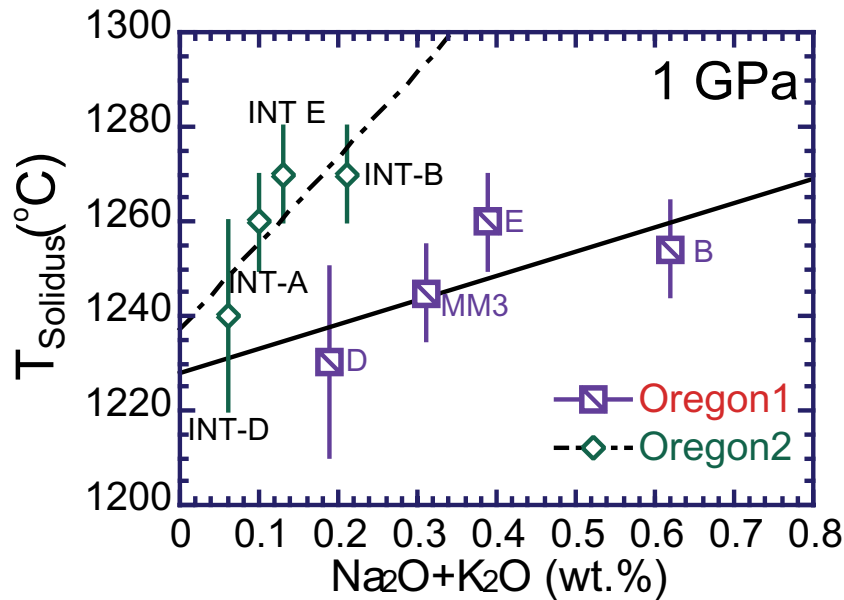


Figure 6. Comparison of extrapolated solidus temperatures for “Oregon1” [Baker *et al.*, 1995; Pickering-Witter and Johnston, 2000] and “Oregon2” [Schwab and Johnston, 2000] experiments at 1 GPa. MM3 solidus is from experimental brackets of Baker *et al.* [1995]; solidi for compositions B, D, and E are extrapolated from melt fraction versus temperature data from the Oregon study of Pickering-Witter and Johnston [2000]. Solidi for Oregon2 compositions are taken from consideration of Schwab and Johnston [2000] data on melt absent conditions (INT-A: 1255°C, INT-E, 1245°C) and on their melt fraction versus temperature trends. Error bars are as in Figure 5. Lines through data are least squares fits that give slopes of 180° and 50°C/wt % alkali with r^2 of 0.54 and 0.67 for the Oregon1 and Oregon2 trends, respectively. Although the former is not statistically distinguishable from a constant value for the solidus and the latter is just barely distinguishable, these positive slopes are expected for arrays of peridotite compositions in which increases in CaO are much greater than increases in alkalis (see text).

2000]. Although not completely accurate, for the sake of brevity these three data sets are hereafter referred to as the Tokyo, Bristol, and Oregon studies. Compositions of key peridotites from these studies are given in Table 3. All of the peridotite compositions from the Tokyo experiments and most of those from the Oregon experiments lack melt-absent constraints, but as described in the previous section and in the captions to Figures 4, 5, and 6, estimates of solidi can be derived from extrapolation of temperature versus melt fraction trends. Melt fractions for the Tokyo experiments have been adjusted using realistic estimates of Na partitioning, as described in the previous section and the captions to Figures 2, 4, and 5.

[16] The experimentally investigated compositions span almost the entire range of Mg # values determined for terrestrial peridotite xenoliths (Figure 3a). Na₂O contents range from 0.06 wt % up to 0.66 wt %, but most cluster near 0.3 wt % and the majority of samples are relatively poor in K, though PHN-1611 has 0.14 wt % K₂O and HK-66 has 0.07 wt % (Table 3). Unfortunately, there is a significant correlation between Mg # and total alkalis for the peridotite compositions used in the 1.5 and 3 GPa experiments considered (Figure 3a). This hampers but does not wholly prevent independent evaluation of the effect of these compositional variables on the solidus.

[17] CaO concentrations of peridotites can be taken as a proxy for cpx mode, although the cpx mode also depends on temperature and pressure of equilibration. For the Tokyo and Bristol bulk compositions, CaO concentrations range only from 2.97 to 3.44 wt % (Figure 3b), but they vary from 2.25 to 8.87 wt % in the Oregon starting materials (Figure 3b). Bulk compositions for the *Pickering-Witter and Johnston* [2000] and *Schwab and Johnston* [2000] experiments plot along distinct trajectories in Figure 3b, as the latter have systematically less alkali at a given CaO content. For convenience, we refer to these distinct compositional paths as the Oregon1 [*Pickering-Witter and Johnston*, 2000] and Oregon2 and [*Schwab and Johnston*, 2000] trends.

[18] We first examine variations in solidi for the Bristol and Tokyo experiments in order to understand the effects of Mg # and of alkali content for samples that differ little in clinopyroxene mode. Solidi at 1.5 GPa differ by 50°C for the Bristol experiments and 80°C for the Tokyo experiments (Figure 4). Total variation for all five compositions is 100°C, though some of this could be attributable to interlaboratory differences. Looking only at the Bristol experiments, MPY has a solidus 50°C cooler than Tinaquillo. Because these two peridotite compositions have similar Mg # values (90.1 versus 90.4) but differ in Na₂O by a factor of 2 (0.4 versus 0.18 wt %), one can infer that alkali content has a greater influence on solidus temperatures than Mg # at this pressure. Solidi for the Tokyo experiments do not show strong correlations with Mg # or total alkalis (Figure 4), in part because the K₂O-rich PHN-1611, which has intermediate Mg # and total alkalis, has a very low solidus temperature. HK-66 has a lower solidus than KLB-1 and based on the trends from the Bristol experiments, this may be owing chiefly to its higher total alkali content rather than its lower Mg #.

[19] The inference that alkalis have a greater influence on the peridotite solidus temperatures than Mg # is supported by experiments on compositions removed from natural peridotites. Comparison of solidi of model spinel peridotite compositions in the systems Na₂O-CaO-MgO-Al₂O₃-SiO₂ and FeO-CaO-MgO-Al₂O₃-SiO₂ show that Na₂O has a much greater effect on solidus temperature than Mg # [*Walter and Presnall*, 1994; *Gudfinnsson and Presnall*, 2000]. Also, as noted by *Herzberg et al.* [2000], the 1.5 GPa solidus of a model Martian peridotite with extraordinarily low Mg # (75) and modest enrichment in Na₂O (0.5 wt %) is 1290 ± 10°C [*Bertka and Holloway*, 1994], similar to natural terrestrial peridotite compositions with Mg # values of near 90 (Figure 4).

[20] Peridotite solidi at 3 GPa for the Bristol and Tokyo experiments are plotted in Figure 5 against Mg # and against bulk alkalis. At this pressure, solidus temperatures for the Bristol and Tokyo experiments correlate with decreasing Mg # and increasing bulk alkalis. The solidus of fertile peridotite KR4003 (Table 3) is consistent with this trend (Figure 5) [*Walter*, 1998]. Taken together, the data suggest a decrease in solidus temperature of 157°C per percent alkalis in the bulk or 13.3°C per decrease in Mg #. The latter is less than the 20°C per Mg # estimate of *Langmuir et al.* [1992], who applied this value to argue that variations in peridotite composition in basalt source regions have relatively small effects on melt production. To the extent that melt production is controlled by solidus location, the trends in Figure 5 support this contention, although it is important to note that solidus location is not the only variable affecting melt production [*Asimow et al.*, 1997; *Hirschmann et al.*, 1999].

[21] The excellent correlations between peridotite bulk composition and solidus temperature at 3 GPa (Figure 5) contrast with the

relatively poor correlations at 1.5 GPa and are surprising, given the possible effects of inter-laboratory uncertainties and considering that bulk alkali wt %, which does not account for the differences in molecular weights of Na₂O and K₂O or for differences in the chemical behavior of the two oxides, is a rather crude index of peridotite enrichment. Thus there may be an element of fortuity in the trends in Figure 5.

[22] Bulk alkali concentrations for the peridotites in the Oregon studies correlate with CaO and cpx mode [Pickering-Witter and Johnston, 2000; Schwab and Johnston, 2000] (Figure 3b). Mg # values are nearly constant at 90.2 ± 0.3 for the Oregon1 compositions and cluster near 90.9 ± 0.1 for the Oregon2 compositions. On the basis of Figures 4b and 5b one might expect solidus temperature to correlate inversely with bulk alkalis. However, in contrast to the Bristol and Tokyo results, solidi of the Oregon compositions extrapolated from experimental temperature-melt fraction trends have weak positive correlations with bulk alkali compositions, if each study is considered separately (Figure 6). Additionally, compared to the Oregon1 trend, the Oregon2 trend, which has a lower alkali/CaO ratio, has higher solidi at a given bulk alkali content and the solidi increase more per increase in bulk alkali concentration. As argued in greater detail below, these observations suggests that bulk alkalis alone do not provide reliable predictions of the relative temperatures of peridotite solidi at any particular pressure and that the relationship between alkali content and modal clinopyroxene influences the solidus significantly.

6. Discussion

[23] The Bristol and Tokyo trends suggest that for peridotites with similar CaO content, solidus temperature is influenced primarily by bulk alkali concentration and, to a lesser

extent, Mg # (Figures 4 and 5). Disturbances to the overall effect of alkalis may be attributable to the different effects of K₂O versus Na₂O. However, the Oregon experiments show that when CaO varies significantly, the effect of alkalis can be reduced or perhaps even reversed (Figure 6). These effects can be explained by relating the solidus temperature of nominally dry peridotite to the composition of the near-solidus liquid. Simply put, near-solidus liquids enriched in minor elements such as alkalis have reduced activities of major components, thereby stabilizing liquid relative to residual minerals. Because near-solidus liquid composition is related to bulk peridotite composition, correlations between solidus temperature and bulk composition may be observed, but complexities in this relationship arise because bulk alkali concentration does not uniquely control near-solidus liquid composition.

6.1. Model Ternary

[24] The relationships described above can be better understood from examination of a model ternary system consisting predominantly of two components, A and B, which form a solid solution (Figure 7a), and a third minor component C, which is assumed to be highly incompatible in the solid solution relative to a ternary A-B-C liquid (Figure 7b). This model was examined in detail by Hirschmann *et al.* [1999], who showed that it has some of the main features necessary to understand the partial melting behavior of natural peridotites. Liquidus isotherms of this system are estimated from a simple cryoscopic (freezing-point depression) relationship. Mineral-liquid exchange of A and B is governed by a single exchange coefficient K_D (assumed to be equal to 0.3) and partitioning of C between liquid and solid is governed by a constant partition coefficient D_C . Additional details of the phase equilibria relationships and the thermodynamic parameters necessary to define this system are

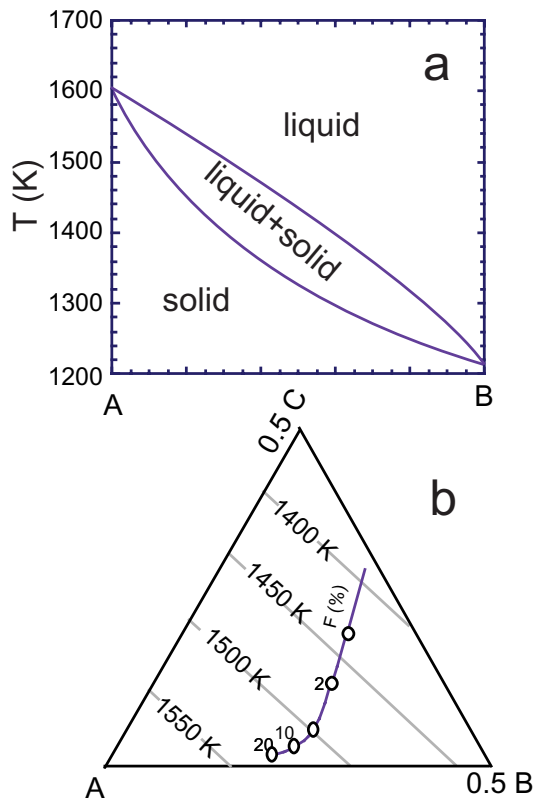


Figure 7. Model A-B-C ternary system used to illustrate the effect of near-solidus liquid composition on solidus temperature. Pure component A is assumed to melt at 1600 K with an enthalpy of fusion of 50 kJ. Mineral-liquid partitioning of A and B is governed by a simple equilibrium constant, $K_D = (X_A^{liq} X_B^{sol} / X_A^{sol} X_B^{liq})$, assumed to be equal to 0.3; partitioning of C is governed by a Nernst partition coefficient D_C . Further details are given by Hirschmann *et al.* [1999]. (a) shows behavior in bounding A-B binary, (b) shows composition-temperature path up to 20% melting for the liquid for values of $D_C = 0.01$ and $X_C = 0.003$, for which a solidus temperature of 1391 K is calculated.

given by Hirschmann *et al.* [1999] and in the caption to Figure 7.

[25] Calculated near-solidus liquids are highly enriched in the incompatible component C (Figure 7b). Such liquids are also enriched in B relative to A owing to the assumed topology

of the A-B binary loop (Figure 7a). Because these effects dilute the amount of component A in the liquid, they depress the liquidus temperature owing to freezing-point depression. We can use these relationships to examine the effects of A-B variations in the system (analogous to variations in Mg # in natural peridotites) relative to variations in C concentrations (analogous to variations in alkali contents). To facilitate this, we define a parameter M , which is equal to $A/(A + B)$. Additionally, we can examine the relative effects of varying bulk C concentration and D_C . Variations in D_C can be thought of either as differences in chemical species (e.g., the more incompatible behavior of K relative to Na), or changes in the bulk D of a particular component, owing either to variations in mode (e.g., higher cpx mode leading to higher values of D_{Na}) or to effects associated with pressure or phase composition (e.g., increased D_{Na} with increasing pressure [Blundy *et al.*, 1995]).

[26] The calculated solidus temperature for the model system with varying M and for different values of D_C are shown as a function of bulk X_C in Figure 8, which illustrates four points that are applicable to experimental results on natural peridotites:

1. The effect of an incompatible element on the solidus depends on its bulk distribution coefficient. Note that the slopes of trends in Figure 8 become steeper with decreasing D_C , so highly incompatible elements can have a marked effect on the solidus, even when they are relatively dilute in the bulk composition. Thus the strong effect of K_2O on peridotite solidi, even at low bulk concentration is owing to the very small value of D_K in peridotite mineral residua.
2. Compared to changes in solid solution composition, as represented by M , incompatible elements have a potent effect on

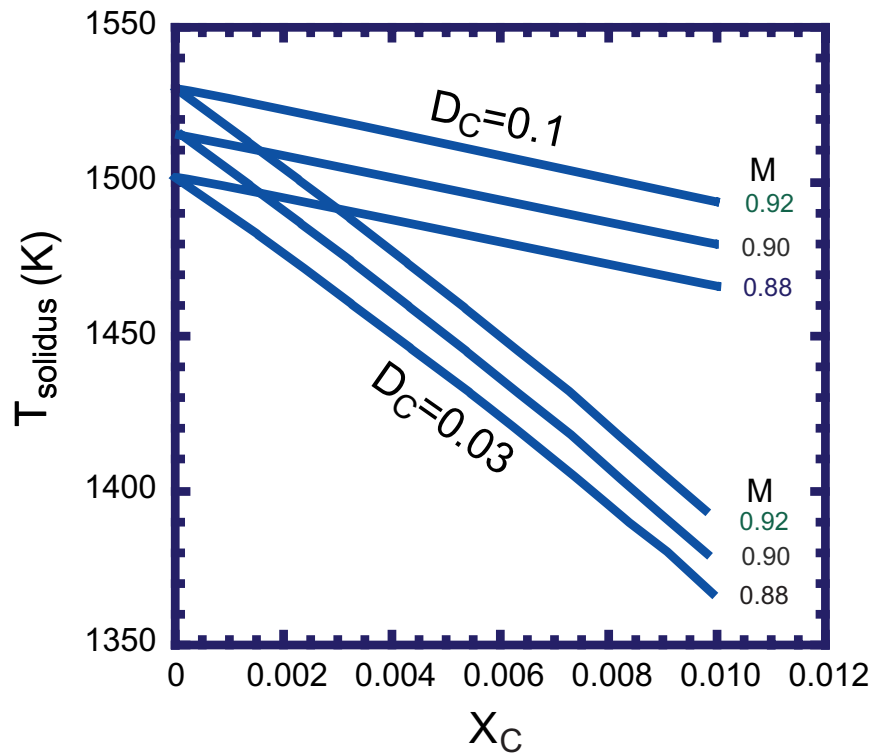


Figure 8. Calculated solidus temperature for model A-B-C ternary depicted in Figure 7, for different values of X_C , D_C , and M ($=A/(A + B)$). When D_C is small (e.g., 0.03), X_C , which is analogous to bulk alkali concentration in natural peridotite, has a strong effect on calculated solidus temperature. When X_C is larger (e.g., 0.1), X_C has less of an effect, and the relative importance of M , which is analogous to Mg # in natural peridotite, is of greater relative importance.

solidus temperatures owing to their strong concentrations in near-solidus liquids. Note that modeled variations in X_C are at the tenth of a percent level, whereas those for M are at the percent level. Although the effect of X_C and M in this simple model are not quantitative indications of peridotite behavior, the order of magnitude of the effects of their variations should be comparable to those of alkalis and Mg # in natural systems.

- Changes in compatibility affect the relative importance of incompatible elements in influencing the solidus temperature. Thus, when C is strongly incompatible ($D_C = 0.03$), variations in X_C are significantly

more important than M variations, but as D_C increases, M variations become more important. Thus it is not surprising that Na_2O is the dominant parameter determining the solidus temperature of peridotite at low pressure, when D_{Na} is small. The strong correlation between solidus temperature and Mg # at 3 GPa may be partly because of the increasing role of Mg # relative to Na_2O , as Na_2O becomes more compatible with increasing pressure [Blundy *et al.*, 1995].

- Because the effect of an element on the solidus temperature is a function of both its abundance in the peridotite and its bulk partition coefficient, variations in mineral

modes that are coupled to changes in peridotite composition may have opposing effects. Thus, in the Oregon trends, variations in bulk Na_2O are offset or even exceeded by those of clinopyroxene mode. *Pickering-Witter and Johnston* [2000] presented a similar explanation for their observed variations in isobaric melt productivity.

6.2. Role of Near-Solidus Liquid Composition

[27] Although the near-solidus liquid compositions for the experiments examined above are not all known precisely, it is possible in some cases to estimate the alkali concentrations in near-solidus liquids from isobaric series of partial melting experiments. For the Bristol and Oregon1 experiments we calculate the alkali concentrations at the solidus ($F = 0$), by extrapolating the experimental trend in alkalis versus melt fraction using the batch melting equation [*Shaw*, 1970] and determining by least squares the bulk D values for Na and K that give the best fit to the experimental data (Figure 9).

[28] For the Bristol experiments (Figure 9a) the inferred near-solidus liquid for MPY has greater alkalis than Tinaquillo, which is consistent with the lower relative solidus for MPY (Figure 4). However, in the Oregon1 experiments the more alkali-rich bulk compositions have greater effective D values for the alkalis owing to higher cpx modes, and therefore near-solidus alkali contents are similar to one another (Figure 9b). Thus the small variations in solidus temperature for the Oregon1 experiments are because their near-solidus liquid compositions are similar. Additionally, alkali concentrations for near-solidus liquids in the Oregon2 experiments correlate inversely with bulk alkali concentrations (Figure 9c), which is consistent with the lower solidus tempera-

tures inferred for more depleted compositions in this series (Figure 6). These observations are consistent with the hypothesis that near-solidus liquid composition has a more direct influence on solidus temperature than bulk composition.

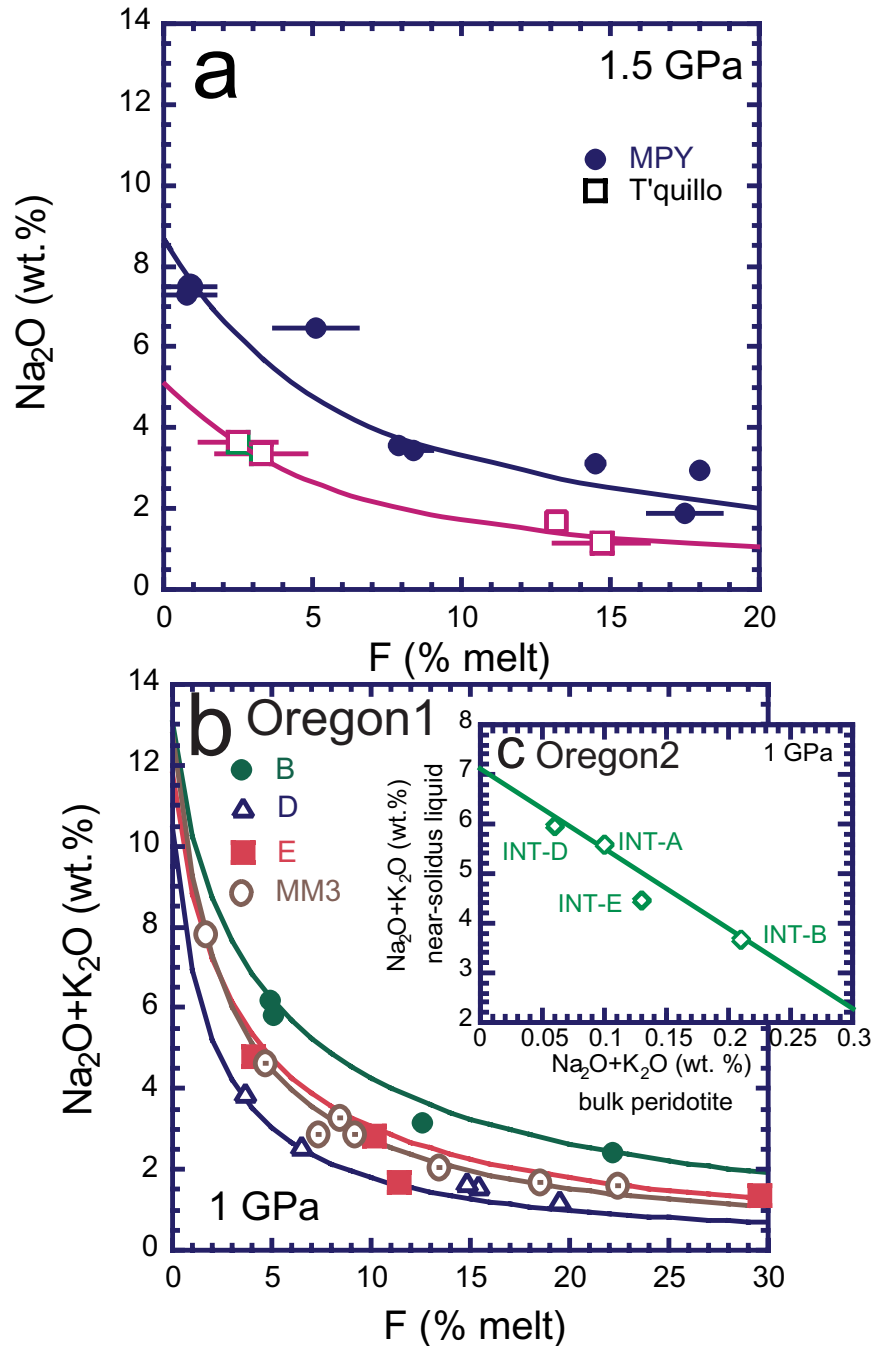
[29] Unfortunately, reconstruction of near-solidus melt composition for the Tokyo experiments based on melt fraction versus liquid composition data would be circular, as melt fractions are estimated from alkali concentrations. However, assuming that $D_K = 0.01$ and $D_{\text{Na}} = 0.05$, then KLB-1, HK-66, and PHN-1611 have increasing alkalis in near-solidus liquids (8.0, 20.2, and 22.3 wt % total alkalis) respectively, in reverse order of their estimated solidus temperatures (e.g., Figures 4, 5). The extreme enrichments in HK-66 and PHN-1611 are in part owing to their high K_2O content. For example, PHN-1611 has 0.14 wt % K_2O , so if $D_K = 0.01$, its near-solidus liquid has 14 wt % K_2O . So, rather modest enhancements in bulk K_2O content can have an extraordinary effect on near-solidus liquid composition and a correspondingly strong effect on solidus temperature.

6.3. Effect of Peridotite Composition, Revisited

[30] As is clear from section 6.1, the effect of compositional variation on the peridotite solidus depends in large part on the competing effects of increased abundance of melt-enhancing components (alkalis, lower Mg #) and the effects of increased compatibility of those components (cpx mode). Thus the common assumption that enriched peridotite melts at lower temperature than normal peridotite may require some modification. Also, the effect of composition must depend on the agent responsible, as different processes have potentially distinct effects on melt-enhancing components and on clinopyroxene mode.

[31] In this context, we return to the relationship between concentrations of CaO and alkalis for different peridotite compositions (Figures 3 and 10). Peridotite compositions in the upper left of

these diagrams, with highest alkalis and lowest cpx mode, are expected to have the lowest solidus temperatures; those in the lower right are expected to have the highest solidi. Among



experimentally studied compositions, distinct trends are apparent. For the Oregon1 and Oregon2 experiments, CaO and alkalis covary and solidus temperatures increase with increasing alkalis (Figure 6), whereas all other compositions reviewed thus far plot along a near-vertical array of variable alkalis at approximately constant CaO and have solidus temperatures that decrease with increasing alkalis (Figures 4b and 5b). One may envision that intermediate between these is a compositional trend along which solidus temperature is constant, which we call the “zero solidus shift” (ZSS) line (Figure 10). Presumably, secular decreases in Mg # with increasing alkali content would cause the ZSS trend to have a shallower slope on this diagram and melting at increased pressures, leading to greater compatibility of Na, would steepen the ZSS. The nearly vertical trend represented by the other peridotite compositions represents the compositional vector corresponding to the range of most experiments on peridotite to date. We therefore call this the “experimental peridotite trend” (EPT). Variation of the solidus along the EPT is similar to that discussed in the text above and depicted in Figures 4 and 5.

[32] The ZSS and EPT can be compared to variations in natural peridotite compositions,

as represented by the compilation of xenoliths from the continental lithosphere by *Herzberg et al.* [1988] (Figure 10). Available peridotite data from other environments (abyssal peridotites, orogenic massifs, etc.) would not appear appreciably different on this plot. Although the natural peridotite compositions are highly variable, it is apparent that most plot along a trend extending from a “typical” fertile composition similar to KLB-1 down to more CaO and alkali-depleted compositions. It is well recognized that this trend is largely owing to extraction of basaltic melts [e.g., *McDonough and Rudnick*, 1998, and references therein], but the key point is that the characteristic slope associated with most natural compositional variation is unlike the EPT. This suggests that variations in solidus temperature for nominally dry natural peridotite compositions should be less pronounced than those indicated by trends such as those depicted in Figures 4 and 5.

[33] Another way to consider the variations in peridotite composition depicted in Figure 10 is to examine the effects of various enrichment processes on peridotite composition and, by inference, on solidus temperature. Although depletion processes such as melt extraction are of considerable interest, available experimental data provide relatively few constraints

Figure 9. Total alkalis in wt % against melt fraction from partial melting experiments of peridotite for (a) the Bristol experiments on MPY, Tinaquillo at 1.5 GPa [*Robinson et al.*, 1998] and (b) the Oregon1 experiments [*Pickering-Witter and Johnston*, 2000] on peridotites with variable mineral modes. Trends are extrapolated to the solidus ($F = 0$) using the batch melting equation [*Shaw*, 1970]. For the Bristol experiments a best fit bulk D_{Na} (0.057, MPY; 0.049, Tinaquillo) is found by least squares to provide the closest agreement with the experiments. For the Oregon experiments, Na_2O and K_2O versus F trends are modeled using published cpx and opx mineral modes and $D_{\text{Na}}^{\text{cpx/liq}}$ and $D_{\text{Na}}^{\text{opx/liq}}$ (0.15 and 0.028) from mineral-liquid data of *Pickering-Witter and Johnston* [2000] and assuming $D_K = 0.01$. A similar trend would be found if fits to these trends were determined by the same least squares method applied to the Bristol experiments. (c, inset) Alkali concentrations of near-solidus liquids for the Oregon2 experiments [*Schwab and Johnston*, 2000] correlate inversely with bulk alkali concentration, which is consistent with the observation that the low-alkali bulk compositions have lower solidus temperatures (Figure 6). Near-solidus liquids for compositions INT-B and INT-E are taken from experiments with melt fractions of 0.1 ± 0.6 and 0.0 ± 0.4 , calculated from mass balance by *Schwab and Johnston* [2000]. Near-solidus liquids for compositions INT-A and INT-D are calculated by the same method and with the same parameters used for the Oregon1 series above.

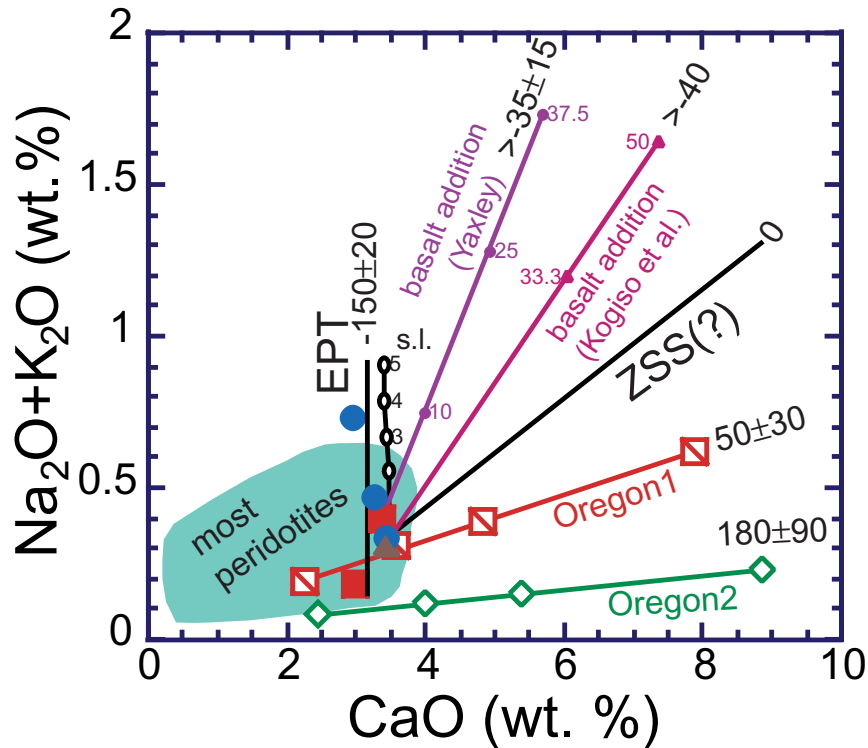


Figure 10. As alkalis increase along the “Oregon1” [Pickering-Witter and Johnston, 2000] and “Oregon2” [Schwab and Johnston, 2000] trends, solidus temperature increases (see Figure 6). As alkalis increase along the experimental peridotite trend (EPT) formed from experimental results on compositions commonly used for peridotite partial melting experiments, solidus temperature decreases (Figures 4 and 5). The zero-solidus shift (ZSS) line marks schematically the hypothetical trend over which solidus temperature remains constant. Also shown are the bulk compositions of peridotite + basalt experiments of Kogiso *et al.* [1999] and Yaxley [2000], with percent basalt added as labeled. The differences in these trajectories are owing to the low CaO (9.5 wt %) of the Yaxley [2000] basalt composition. Italicized numbers next to experimental trends and the ZSS are the change in solidus temperature per percent alkalis added, with the value for the EPT taken at 3 GPa (Figure 5) and values for the Oregon experiments from Figure 6. Also shown is the hypothetical compositional effect of addition of siliceous alkali-rich liquid (1.5 wt % CaO, 12 wt % Na₂O + K₂O) similar to glasses trapped in peridotitic minerals [Schiano and Clocchiatti, 1994]. Tick marks along liquid addition lines are 1% liquid addition. Field marked “most peridotites” is from peridotite xenolith compositions from Herzberg *et al.* [1988]; compare with similar field in Figure 3. Symbols are as in Figure 3.

on these effects (but see Hirose and Kushiro [1998]). On the other hand, several distinct enrichment processes may be examined, including enrichment by addition of a basaltic component [e.g., Tabit *et al.*, 1997; Kogiso *et al.*, 1999; Yaxley, 2000] or metasomatism by an alkali-rich, silica-rich fluid similar to those found trapped in melt inclusions in peridotitic

minerals from many localities [e.g., Schiano and Clocchiatti, 1994].

[34] Addition of basalt to peridotite causes a relatively small shift in the alkali concentrations and CaO contents of peridotite (Figure 10) and therefore is expected to affect the solidus less than the EPT for a given increment

of alkalis added. This inference is consistent with available experimental data on partial melts of peridotite/basalt hybrids. For example, KLB-1 peridotite/basalt hybrids with ratios of 67/33 and 50/50 and 1.2 and 1.64 wt % Na₂O + K₂O respectively have melt fraction versus temperature trends at 1.5, 2, and 3 GPa that suggest only small decreases (<50°C) in solidus temperature relative to pure KLB-1 [Kogiso *et al.*, 1999]. Also, Yaxley [2000] bracketed the solidus at 3.5 GPa of a 75/25 MPY peridotite/basalt mixture having 1.28 wt % Na₂O + K₂O and found it to be $\leq 50^\circ\text{C}$ lower than pure MPY-90.

[35] The increase in cpx mode that accompanies basalt addition must be partly responsible for the small, observed effect of basalt addition on peridotite solidus temperature. Differences between the basalt addition trend and the EPT and these experimental results suggest that the EPT is not a good analogue for the effects on peridotite of refertilization by basalt. However, it remains somewhat surprising that the solidus decrease associated with the basalt addition experiments of Kogiso *et al.* [1999] at 3 GPa and Yaxley [2000] at 3.5 GPa is so much less-pronounced than the 3 GPa EPT. More specifically, the Yaxley [2000] basalt addition trend is colinear with the Bristol MPY and Tinaquillo compositions in Figure 10; however, while the data of Yaxley [2000] suggest that alkalis decrease the solidus by $30 \pm 15^\circ\text{C}/\text{wt } \%$, the Bristol data indicate $200^\circ\text{C}/\text{wt } \%$. If anything, one might expect greater solidus depression from basalt addition, as it is accompanied by increases in K₂O and large decreases in Mg #, whereas MPY and Tinaquillo have no K₂O and nearly identical Mg # values [Robinson and Wood, 1998]. Increases in Al₂O₃ per increment CaO are equivalent for the two sets of bulk compositions [Robinson and Wood, 1998; Yaxley, 2000] and Cr₂O₃, which may tend to increase solidus temperature [Herzberg *et al.*, 2000] increases with increasing CaO for the

peridotites (Table 3) but decreases for the basalt addition experiments [Yaxley, 2000]. One feature that might provide a partial explanation is that Tinaquillo is in the spinel peridotite facies at 3 GPa, whereas MPY [Robinson and Wood, 1998] and all of the Yaxley [2000] compositions are in the garnet peridotite facies, but this seems unlikely to account for all of the difference. On the other hand, the Robinson and Wood [1998] experiments used the sandwich technique, which could compromise both their solidus determinations and the placement of the Bristol compositions on Figure 10 (and also, unfortunately, on Figures 3, 4, and 5). Yaxley [2000] used direct melting experiments, which also has potential pitfalls, as noted above. More experimental work will be required to reconcile the basalt addition experiments with experimentally observed compositional effects on peridotite melting behavior.

[36] In contrast to basalt, just a few percent of alkali-rich, siliceous liquids similar to glasses trapped in peridotitic mineral inclusions would cause alkali enrichment comparable to the span of the EPT and accompanied by CaO depletion (Figure 10). Thus, in contrast to the relatively subdued effects of basalt addition, metasomatism by 3–4 wt % siliceous melt could lower the peridotite solidus by 100°C or more. Because siliceous melt inclusions in peridotites are commonly volatile-rich [Schiano and Clocchiatti, 1994], even greater effects are likely. Also, though addition of basalt may have a modest effect on the peridotite solidus, the effect of a silicic, alkali-rich, CaO-poor partial melt of basalt (e.g., from pyroxenitic heterogeneities [Yaxley and Green, 1998; Pertermann and Hirschmann, 1999]) may be considerably larger.

6.4. Recommended Solidus

[37] The parameterization of the complete data set of peridotite solidus constraints performed at the outset of this paper does not account for

the effects of interlaboratory uncertainties or the effects of composition. The problem of interlaboratory uncertainties will remain until unambiguous methods for solidus determination are widely applied and until authoritative calibration and standardization of temperature and pressure measurements are adopted. It is worth noting that the last interlaboratory pressure calibration in piston-cylinder devices was >25 years ago [Johannes *et al.*, 1971] using pressure assemblies unlike the BaCO₃ and CaF₂ salt cells in common use in many contemporary experimental laboratories. No similar interlaboratory calibration has been performed for multianvil devices. Temporarily, it is deemed best to treat the scatter in Figure 1 that may be attributable to interlaboratory uncertainty as a random error.

[38] Compositional effects, while not understood quantitatively as a function of all possible variables and as a function of pressure, are sufficiently well constrained to allow some filtering of the data. Those compositions that are enriched in alkali/cpx modal ratio or enriched in K₂O relative to typical upper mantle peridotite are likely to have solidi that are lower than that of typical mantle. There are many estimates for the composition of peridotite in various source regions but a conservative filter to apply is to exclude all compositions substantially more enriched than primitive upper mantle (0.36 wt % Na₂O, 19% cpx, 0.03 wt % K₂O [McDonough and Rudnick [1998]]. Some regions of the convecting mantle, such as the MORB source region, could be more depleted than this. From the post-1988 database (Table 1), enriched peridotite compositions include HK-66 (0.66 wt % Na₂O, 0.09 wt % K₂O [Hirose and Kushiro, 1993]), PHN-1611 (0.33 wt % Na₂O, 0.14 wt % K₂O [Kushiro, 1996]), HPY from experiments of Falloon and Green [1988] and Falloon *et al.* [1988] (0.57 wt % Na₂O; 0.13 wt % K₂O) and KR4003 (0.22 wt % Na₂O,

0.09 wt % K₂O [Walter, 1998]). Also, it seems reasonable to exclude depleted compositions that may have elevated solidi, such as Tinaquillo from the experiments of Robinson and Wood [1998] and Robinson *et al.* [1998] (0.18 wt % Na₂O, 0.00 wt % K₂O), and the Oregon2 compositions of Schwab and Johnston [2000].

[39] The best fit to the post-1988 database with the enriched and depleted compositions removed is given by $aP^2 + bP + c$ with $a = -5.904$, $b = 139.44$, $c = 1108.08$ (Table 2). Although it is impossible to determine formal uncertainties, the overall agreement between experimental constraints combined with knowledge of experimental uncertainties suggest that this fit may be accurate to within $\pm 20^\circ$, $\pm 35^\circ$, and $\pm 50^\circ\text{C}$ over the pressure intervals 0–3.5, 3.5–6.5, and 6.5–10 GPa. Interestingly, this fit using filtered data is not very different from the preliminary fit for the post-1988 data found above; the data-filtered fit is 25°C hotter at 1 bar and 20°C hotter at 10 GPa but is within 10°C of the preliminary fit over much of the pressure interval considered (Figure 12).

6.5. Comparison of the Recommended Peridotite Solidus to Previous Models

[40] Parameterization of the peridotite solidus plays a key role in models of partial melting of the mantle. Two widely used such parameterizations are that of McKenzie and Bickle [1988] and Langmuir *et al.* [1992], which are based on the same pre-1988 compilation of peridotite solidus experiments from McKenzie and Bickle [1988]. Also, Iwamori *et al.* [1995] parameterized the peridotite solidus based on a more restricted set of experiments and most recently Herzberg *et al.* [2000] proposed a solidus based primarily on experiments on KLB-1 peridotite. As illustrated in Figure 12, the new parameterization is similar to that pro-

posed by *Langmuir et al.* [1992] below 2 GPa but cooler at higher pressures, with differences increasing to a maximum of 55°C at 4 GPa. The *Langmuir et al.* [1992] parameterization is based on data up to 3.5 GPa but was applied by them up to 4 GPa. Compared to the parameterization of *McKenzie and Bickle* [1988], the new parameterization is slightly hotter below 2 GPa, cooler between 2 and 6.5 GPa, and hotter above 6.5 GPa (Figure 12). A maximum difference of 43°C occurs near 4.3 GPa. Differences between the recommended fit with the solidus of *Iwamori et al.* [1995] vary with pressure; the Iwamori et al. solidus is at least 30° hotter between 3 and 6 GPa, reaching a maximum difference of 65°C, and markedly cooler above 7.5 GPa. The latter difference is probably less significant, given the large unresolved discrepancies in high-pressure solidus determinations (Figure 11). The KLB-1-based peridotite solidus of *Herzberg et al.* [2000] is nearly identical to the preferred fit in the pressure intervals of 0–3 and 5–10 GPa but is 20°–33°C hotter between 3 and 5 GPa.

[41] A salient feature of these comparisons is that the preferred solidus is 20°–65°C cooler than other parameterizations between 3 and 6.5 GPa. This difference stems in part from incorporation here of newer experimental constraints. Also, in comparison to the recent *Herzberg et al.* [2000] KLB-1-based solidus, the present fit may be depressed to lower temperatures owing to incorporation of experimental data from the slightly enriched MPY composition (Table 3, Figure 3). However, alternative fits that exclude MPY and similar compositions differ from the preferred fit by no more than 15°C (Table 3, Figure 12), about half the difference between the present model and *Herzberg et al.* [2000]. Additionally, some of the differences between experimental results on MPY and similar compositions and those more like KLB-1 are likely owing to experimental uncertainties.

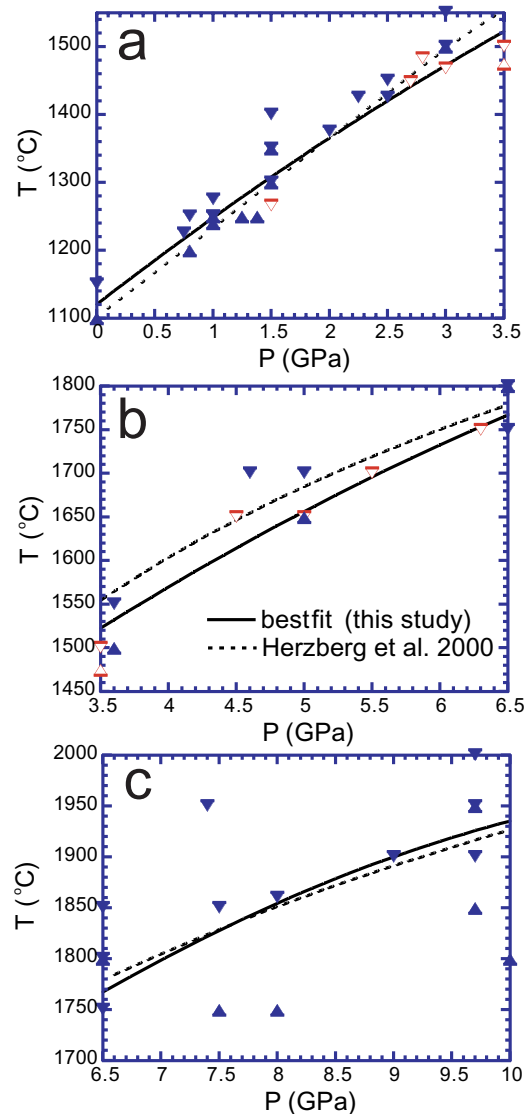


Figure 11. Constraints on peridotite solidus location from post-1988 data (Table 1) excluding enriched and depleted compositions as described in the text, compared to the preferred peridotite solidus (solid line) over the temperature intervals (a) 0–3.5, (b) 3.5–6.5, and (c) 6.5–10 GPa. Arrows pointing up are melt-absent experiments, those pointing down are melt-present experiments. Open arrows are experiments on MPY peridotite (and also, KH80-100 [Canil, 1992], which is similar to MPY). Also shown for comparison is the peridotite solidus proposed by *Herzberg et al.* [2000] (dotted line).

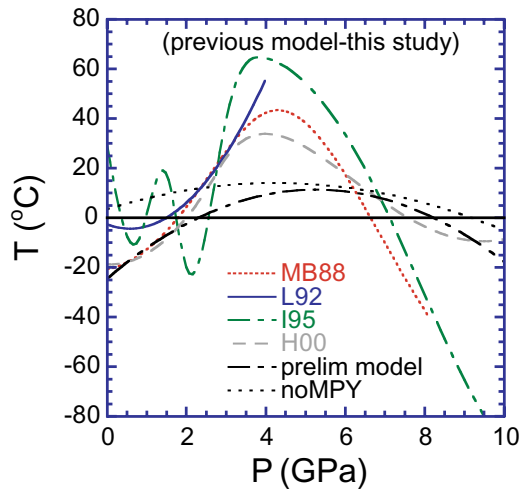


Figure 12. Comparison of recommended peridotite solidus, derived from peridotite data with enriched and depleted compositions excluded, relative to selected other model solidi from *McKenzie and Bickle* [1988] (MB88), *Langmuir et al.* [1992] (L92), *Iwamori et al.* [1995] (I95) and *Herzberg et al.* [2000] (H2000). The plotted parameter is the difference between the solidus temperature of the previous model and that of the preferred best fit from this study. Thus a value greater than zero on this graph indicates that the previous model is hotter than the proposed best fit solidus. Also shown is the difference between the preliminary solidus from Figure 1, which was derived from data not filtered for enriched and depleted compositions and the recommended solidus. The difference between an alternative fit (Table 3) to the solidus with MORB-pyrolite and similar compositions excluded and the best fit model is also shown.

[42] These differences have small but not inconsequential effects on partial melting models. For example, mantle adiabats that would encounter the solidus at 3 and 4 GPa according to *Langmuir et al.* [1992] would encounter it at 3.3 and 4.6 GPa, respectively, according to the new fit (assuming a mantle adiabat of 10°C/GPa). The maximum difference corresponds to a difference in solidus depth of ~ 20 km. Also, the shallower solidus slope of the present model, if used

as an input parameter to adiabatic melt production models [e.g., *Langmuir et al.*, 1992; *Iwamori et al.*, 1995] leads to lower calculated partial melt productivities. Thus, if the partial melting model of *Langmuir et al.* [1992] is used with the new solidus relation, calculated partial melt productivity near 4 GPa decreases from 15%/GPa to <11%/GPa. For the same adiabat the lower productivity implied by the recommended fit relative to the *Langmuir et al.* [1992] parameterization partially compensates for the deeper onset of melting, although more precise data for melt production are required to rigorously evaluate the effect of the revised solidus on melt production during adiabatic upwelling [e.g., *Asimow et al.*, 1997]. Also, for melting initiated at pressures greater than 3 GPa, we expect a small, predicted increase in the average depth of melting. Finally, the range of potential temperatures required to explain variability in the depth of initial melting in the global mid-ocean ridge system is reduced by $\sim 40^\circ$, as intersection of the solidus at ~ 150 km beneath Iceland, as suggested by models and seismic observations [*Langmuir et al.*, 1992; *Ito et al.*, 1999] occurs at lower potential temperature.

7. Conclusions

[43] The solidus of nominally dry peridotite is constrained by a large number of experimental data between 0 and 10 GPa, and constraints are particularly abundant below 3.5 GPa, but the solidus location remains imperfectly constrained owing to interlaboratory uncertainties and to the effects of compositional variability. Although recent studies allow improved understanding of the effects of peridotite composition on solidus location, interlaboratory uncertainties remain significant. Compositional effects can be minimized by filtering the data for compositions enriched in alkalis.

[44] Bulk peridotite composition influences the solidus temperature indirectly, through its effect on near-solidus liquid composition. Specifically, increased bulk alkalis and decreased Mg # and cause near-solidus liquids to be enriched in fluxing components (alkalis, FeO*). Increased CaO, corresponding to increased clinopyroxene mode, diminishes the enrichment of alkalis in near-solidus liquid; at constant bulk alkali content this has the effect of increasing the solidus temperature. Because the array of peridotite compositions used for most partial melting experiments differs significantly in alkalis but little in CaO, inferences about the effect of peridotite composition on solidus temperature will tend to exaggerate the effect expected relative to what may be the actual variations in the mantle.

[45] The chief difference between the new solidus constrained from compositionally filtered data differs from solidi in common use is that it is at cooler temperatures over the pressure range of 2–6 GPa, with a maximum difference of $\sim 65^{\circ}\text{C}$ near 4 GPa. There are also significant disagreements at pressures approaching 10 GPa, but these largely reflect sparsity of accurate constraining data at these higher pressures.

Acknowledgments

[46] Thanks to Vincent Salters and Jon Blundy for inviting me to contribute a review of the peridotite solidus and its relation to near-solidus liquids for their winter 1999 AGU special session on melting near the peridotite solidus. If they had not asked me to think about the problem, I never would have written this paper. Also, much of the consideration of the “Oregon” data here is an attempt to answer a question that Jon asked in that session. Thanks also to J. Pickering-Witter, B. Schwab, and C. Herzberg for providing preprints that influenced the substance of this paper. This paper benefited from constructive reviews by A. D. Johnston, J. Blundy, and D. Presnall. This work supported by the National Science Foundation OCE 9876255.

References

- Agee, C. B., J. Li, M. C. Shannon, and S. Circone, Pressure-temperature phase diagram for the Allende Meteorite, *J. Geophys. Res.*, **100**, 17,725–17,740, 1995.
- Asimow, P. D., M. M. Hirschmann, and E. M. Stolper, An analysis of variations in isentropic melt productivity, *Philos. Trans. R. Soc. London Ser. A*, **355**, 255–281, 1997.
- Asimow, P. D., M. M. Hirschmann, and E. M. Stolper, Calculation of peridotite partial melting from thermodynamic models of minerals and melts, IV, Adiabatic decompression and the composition and mean properties of mid-ocean ridge basalts, *J. Petrol.*, in press, 2000.
- Baker, M. B., and E. M. Stolper, Determining the composition of high-pressure mantle melts using diamond aggregates, *Geochim. Cosmochim. Acta*, **58**, 2811–2827, 1994.
- Baker, M. B., M. M. Hirschmann, M. S. Ghiorso, and E. M. Stolper, Compositions of near-solidus peridotite melts from experiments and thermodynamic calculations, *Nature*, **375**, 308–311, 1995.
- Bertka, C. M., and J. R. Holloway, Anhydrous partial melting of an iron-rich mantle, I, Subsolidus phase assemblages and partial melting phase relations at 10 to 30 kbar, *Contrib. Mineral. Petrol.*, **115**, 313–322, 1994.
- Blundy, J. D., T. J. Falloon, B. J. Wood, and J. A. Dalton, Sodium partitioning between clinopyroxene and silicate melts, *J. Geophys. Res.*, **100**, 15,501–15,515, 1995.
- Canil, D., Orthopyroxene stability along the peridotite solidus and the origin of cratonic lithosphere beneath Southern Africa, *Earth. Planet. Sci. Lett.*, **111**, 83–95, 1992.
- Falloon, T. J., and D. H. Green, Anhydrous partial melting of peridotite from 8 to 35 kb and the petrogenesis of MORB, *J. Petrol., Lithosphere Issue*, 379–414, 1988.
- Falloon, T. J., D. H. Green, C. J. Hatton, and K. L. Harris, Anhydrous partial melting of a fertile and depleted peridotite from 2 to 30 Kb and application to basalt petrogenesis, *J. Petrol.*, **29**, 1257–1282, 1988.
- Falloon, T. J., D. H. Green, L. V. Danyushevsky, and U. H. Faul, Peridotite melting at 1.0 and 1.5 GPa: An experimental evaluation of techniques using diamond aggregates and mineral mixes for determination of near-solidus melts, *J. Petrol.*, **40**, 1343–1375, 1999.
- Galer, S. J., and R. K. O’Nions, Magmagenesis and the mapping of chemical and isotopic variations in the mantle, *Chem. Geol.*, **56**, 45–61, 1986.
- Gudfinnsson, G. H., and D. C. Presnall, Melting behaviour of model lherzolite in the system CaO-MgO-Al₂O₃-FeO at 0.7–2.8 GPa, *J. Petrol.*, **41**, 1241–1269, 2000.

- Herzberg, C., M. Feigenson, C. Skuba, and E. Ohtani, Majorite fractionation recorded in the geochemistry of peridotites from South Africa, *Nature*, 332, 823–826, 1988.
- Herzberg, C., P. Raterron, and J. Zhang, New experimental observations on the anhydrous solidus for peridotite KLB-1, *Geochem. Geophys. Geosyst.*, in press, 2000.
- Hirose, K., and I. Kushiro, Partial melting of dry peridotites at high pressures: Determination of compositions of melts segregated from peridotite using aggregates of diamond, *Earth. Planet. Sci. Lett.*, 114, 477–489, 1993.
- Hirose, K., and I. Kushiro, The effect of melt segregation on polybaric mantle melting: Estimation from the incremental melting experiments, *Phys. Earth Planet. Int.*, 107, 111–118, 1998.
- Hirschmann, M. M., M. B. Baker, and E. M. Stolper, The effect of alkalis on the silica content of mantle-derived magmas, *Geochim. Cosmochim. Acta*, 62, 883–902, 1998.
- Hirschmann, M. M., M. S. Ghiorso, P. D. Asimow, and E. M. Stolper, Calculation of peridotite partial melting from thermodynamic models of minerals and melts, III, Controls on isobaric melt productivity and the effect of water on melt, *J. Petrol.*, 40, 831–851, 1999.
- Holloway, J. R., Graphite-melt equilibria during mantle melting: Constraints on CO₂ in MORB magmas and the carbon content of the mantle, *Chem. Geol.*, 147, 89–97, 1998.
- Hirth, G. H., and D. L. Kohlstedt, Water in the oceanic upper mantle: Implications for rheology, melt extraction, and evolution of the lithosphere, *Earth. Planet. Sci. Lett.*, 144, 93–108, 1996.
- Ito, G., Y. Shen, G. Hirth, and C. J. Wolfe, Mantle flow, melting, and dehydration of the Iceland mantle plume, *Earth. Planet. Sci. Lett.*, 16, 81–96, 1999.
- Iwamori, H., D. McKenzie, and E. Takahashi, Melt generation by isentropic mantle upwelling, *Earth. Planet. Sci. Lett.*, 134, 253–266, 1995.
- Johannes, W., P. M. Bell, H. K. Mao, A. L. Boettcher, D. W. Chipman, J. F. Hays, R. C. Newton, and F. Seifert, An Interlaboratory comparison of piston-cylinder pressure calibration using the albite-breakdown reaction, *Contrib. Mineral. Petrol.*, 32, 24–38, 1971.
- Karato, S., and H. Jung, Water, partial melting and the origin of the seismic low velocity and high attenuation zone in the upper mantle, *Earth. Planet. Sci. Lett.*, 158, 193–207, 1998.
- Kogiso, T., K. Hirose, and E. Takahashi, Melting experiments on homogeneous mixtures of peridotite and basalt: Application to the genesis of ocean island basalts, *Earth. Planet. Sci. Lett.*, 162, 45–61, 1999.
- Kushiro, I., Partial melting of a fertile mantle peridotite at high pressure and experimental study using aggregates of diamond, in *Earth Processes: Reading the Isotopic Clock*, *Geophys. Monogr. Ser.*, vol. 95, edited by A. Basu and S. Hart, pp. 109–122, AGU, Washington, D. C., 1996.
- Langmuir, C. H., E. M. Klein, and T. Plank, Petrological systematics of mid-ocean ridge basalts: Constraints on melt generation beneath ocean ridges, in *Mantle Flow and Melt Generation at Mid-Ocean Ridges*, *Geophys. Monogr. Ser.*, vol. 71, edited by J. P. Morgan, D. K. Blackmun, and J. M. Sinton, pp. 183–280, AGU, Washington, D. C., 1992.
- Longhi, J., The anhydrous mantle solidus? New experiments in CMAS, *Eos Trans. AGU*, 79(45), Fall Meet. Suppl., F1005, 1998.
- McDonough, W. F., and R. L. Rudnick, Mineralogy and composition of the upper mantle, *Rev. Mineral.*, 37, 139–164, 1998.
- McKenzie, D., The generation and compaction of partial melts, *J. Petrol.*, 25, 713–765, 1984.
- McKenzie, D., and M. J. Bickle, The volume and composition of melt generated by extension of the lithosphere, *J. Petrol.*, 29, 625–679, 1988.
- Pertermann, M., and M. M. Hirschmann, Partial melting experiments on a MORB-like pyroxenite at 3.0 GPa and 1300–1500°C, *Eos Trans. AGU*, 80(46), Fall Meet. Suppl., F1112, 1999.
- Pickering-Witter, J. M., and A. D. Johnston, The effects of variable mineral proportions on the melting systematics of fertile peridotitic assemblages, *Contrib. Mineral. Petrol.*, in press, 2000.
- Pickering-Witter, J., and C. E. Lesher, Melting systematics of a clinopyroxene-rich peridotite at 3.6 GPa, *Eos Trans. AGU*, 80(46), Fall Meet. Suppl., F1125, 1999.
- Plank, T., and C. H. Langmuir, Effects of the melting regime on the composition of the oceanic crust, *J. Geophys. Res.*, 97, 19,749–19,770, 1992.
- Presnall, D., The geometrical analysis of partial fusion, *Am. J. Sci.*, 267, 1178–1194, 1969.
- Robinson, J. A. C., and B. J. Wood, The depth of the spinel to garnet transition at the peridotite solidus, *Earth. Planet. Sci. Lett.*, 164(1–2), 277–284, 1998.
- Robinson, J. A. C., B. J. Wood, and J. D. Blundy, The beginning of melting of fertile and depleted peridotite at 1.5 GPa, *Earth. Planet. Sci. Lett.*, 155, 97–111, 1998.
- Schiano, P., and R. Clocchiatti, Worldwide occurrence of silica-rich melts in sub-continental and sub-oceanic mantle minerals, *Nature*, 368, 621–624, 1994.
- Schwab, B. E., and A. D. Johnston, Melting systematics of modally variable, compositionally intermediate peridotite the effects of mineral fertility, *J. Petrol.*, in press, 2000.
- Shen, Y., and D. W. Forsyth, Geochemical constraints on

- initial and final depths of melting beneath mid-ocean ridges, *J. Geophys. Res.*, **100**, 2211–2237, 1995.
- Shaw, D. M., Trace element fractionation during anatexis, *Geochim. Cosmochim. Acta.*, **34**, 237–242, 1970.
- Soulard, H., and B. J. Wood, Lherzolite partial melting: closer to primary liquids, *Min. Mag.*, **58A**, 866–867, 1994.
- Tabit, A., J. Kornprobst, and A. B. Woodland, Les Peridotites a grenat du massif des Beni Bousera (Maroc): Melanges tectoniques et interdiffusion du fer et du magnésium, *C. R. Acad. Sci., Ser. II.*, **325**, 665–670, 1997.
- Takahashi, E., T. Shimazaki, Y. Tsuzaki, and H. Yoshida, Melting study of a peridotite KLB-1 to 6.5 GPa, and the origin of basaltic magmas, *Philos. Trans. R. Soc. London, Ser. A*, **342**, 105–120, 1993.
- Walker, D., C. B. Agee, and Y. Zhang, Fusion curve slope and crystal/liquid buoyancy, *J. Geophys. Res.*, **93**, 313–323, 1988.
- Walter, M. J., Melting of garnet peridotite and the origin of komatiite and depleted lithosphere, *J. Petrol.*, **39**, 29–60, 1998.
- Walter, M. J., and D. C. Presnall, Melting behavior of simplified lherzolite in the system CaO-MgO-Al₂O₃-SiO₂-Na₂O from 7 to 35 kbar, *J. Petrol.*, **35**, 329–359, 1994.
- Yaxley, G. M., Experimental study of the phase and melting relations of homogeneous basalt + peridotite mixtures and implications for the petrogenesis of flood basalts, *Contrib. Mineral. Petrol.*, **139**, 326–338, 2000.
- Yaxley, G. M., and D. H. Green, Reactions between eclogite and peridotite: Mantle refertilization by subduction of oceanic crust, *Schweiz. Mineral. Perogr. Mitt.*, **78**, 243–255, 1998.
- Zhang, J., and C. Herzberg, Melting experiments on anhydrous peridotite KLB-1 from 5.0 to 22.5 GPa, *J. Geophys. Res.*, **99**, 17,729–17,742, 1994.